

Movement Primitive Diffusion: Learning Gentle Robotic Manipulation of Deformable Objects

Paul Maria Scheikl¹, Nicolas Schreiber², Christoph Haas², Niklas Freymuth²,
Gerhard Neumann², Rudolf Lioutikov², and Franziska Mathis-Ullrich¹

Abstract—Policy learning in robot-assisted surgery (RAS) lacks data efficient and versatile methods that exhibit the desired motion quality for delicate surgical interventions. To this end, we introduce Movement Primitive Diffusion (MPD), a novel method for imitation learning (IL) in RAS that focuses on gentle manipulation of deformable objects. The approach combines the versatility of diffusion-based imitation learning (DIL) with the high-quality motion generation capabilities of Probabilistic Dynamic Movement Primitives (ProDMPs). This combination enables MPD to achieve gentle manipulation of deformable objects, while maintaining data efficiency critical for RAS applications where demonstration data is scarce. We evaluate MPD across various simulated and real world robotic tasks on both state and image observations. MPD outperforms state-of-the-art DIL methods in success rate, motion quality, and data efficiency.

Project page: scheiklp.github.io/movement-primitive-diffusion

Index Terms—Surgical Robotics; Laparoscopy; Imitation Learning; Score-based Diffusion Policies; Movement Primitives

I. INTRODUCTION

ADVANCING the level of autonomy in Robot-Assisted Surgery (RAS) requires novel methods for training policies that satisfy the special requirements of surgical applications. RAS requires the policies to exhibit gentle manipulation of delicate tissue and perform with limited data as human demonstrations are costly. Additionally, human behavior is inherently multimodal [1], covering multiple distinct strategies for solving the same task. Imitation Learning (IL) methods that are unable to represent multimodal behavior may exhibit harmful behavior through mode averaging that is unacceptable in surgical settings, *e.g.*, by averaging over two distinct strategies of dissecting tissue and thus damaging healthy tissue. Diffusion-based Imitation Learning (DIL) has shown to perform well on high-dimensional action spaces, generate multimodal behaviors, and exhibit strong training stability [2], [3], making it a promising framework for application in RAS.

Manuscript received: December 12, 2023; Revised February 23, 2024; Accepted March 18, 2024. This paper was recommended for publication by Editor Pietro Valdastri upon evaluation of the Associate Editor and Reviewers' comments. This work was supported by the Erlangen National High Performance Computing Center funded by the German Research Foundation (DFG), the HoreKa supercomputer funded by the Ministry of Science, Research and the Arts Baden-Württemberg and by the Federal Ministry of Education and Research, and the DFG – 448648559.

¹ P. M. Scheikl and F. Mathis-Ullrich are with the Department Artificial Intelligence in Biomedical Engineering, Friedrich-Alexander-University Erlangen-Nürnberg, 91054 Erlangen, Germany.

Corresponding author: franziska.mathis-ullrich@fau.de
² N. Schreiber, C. Haas, N. Freymuth, G. Neumann, and R. Lioutikov are with the Institute for Anthropomatics and Robotics, Karlsruhe Institute of Technology, 76131 Karlsruhe, Germany.

Digital Object Identifier (DOI): see top of this page.

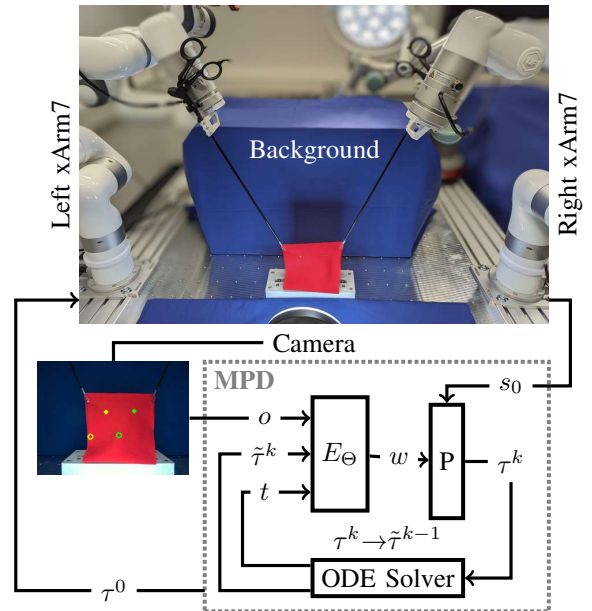


Fig. 1: Schematic for action sequence generation with MPD for bimanual tissue manipulation. Observations o and initial values s_0 for position and velocity are captured on the bimanual robotic setup. An ODE solver solves the Probability Flow ODE with learnable model E_Θ and ProDMP P by iteratively denoising an action sequence $\tilde{\tau}^k$ for diffusion step k and respective noise level t . The final denoised action sequence τ^0 is executed on the robots.

DIL methods train large neural networks to iteratively denoise action sequences drawn from a prior Gaussian distribution to generate motion conditioned on observations. We propose to add temporal correlations between actions during motion generation by utilizing Movement Primitives (MPs) to address both gentle manipulation of deformable objects and data efficiency in DIL. In other methods, neural networks output actions sequences directly [2], [3]. In our proposed method, Movement Primitive Diffusion (MPD), the neural network outputs parameters of a MP that encode a denoised action sequence. These parameters are decoded into smooth position trajectories to enable gentle manipulation of deformable objects.

Leveraging both MPs and DIL, MPD provides a novel approach with increased data efficiency and generation of action sequences that are suitable for gentle deformable object manipulation in RAS. MPD, generates gentle motions that outperform state-of-the-art DIL methods in terms of success rate, motion quality, and required training data. MPD enables generating action sequences with guaranteed initial conditions

for position and velocity, and benefits from a modern diffusion framework for fast inference times. MPD works well for both state observations, as well as raw RGB image observations, which is a critical aspect for application in RAS, as image observations are the only readily available source of information [4]. An overview of action sequence generation with MPD is illustrated in Figure 1.

II. RELATED WORK

Deformable object manipulation in surgery is explored through either modeling deformations or predicting action sequences. Learning deformation models typically offers better generalization by capturing object properties rather than task-specific movements [5]. However, these models commonly only learn the deformation behavior and not the behavior that is required to solve a task [6]. They are thus not applicable to tasks that require complex motions that do not directly deform the object, for example grasping. Model-based strategies are effective for known goal configurations of deformable objects [5] or when deformation involves visual servoing of identifiable landmarks [6]. However, in actual surgical scenarios, where goal configurations and landmarks are uncertain and grasping deformable objects is crucial, these approaches may not suffice. Consequently, our research prioritizes action sequence prediction to address diverse surgical tasks involving grasping, manipulation of deformable objects, and precise motion skills.

Tissue manipulation is a common surgical task that encompasses both direct and indirect manipulation of deformable objects. Examples for direct manipulation are tissue retraction to visualize occluded structures [4], [7], [8] or organ manipulation to bring a deformable object into a desired shape [5], [9]. Indirect manipulation involves moving specific landmarks on tissue by altering the tissue’s shape through manipulation of other points on the tissue. Shin et al. [6] investigate IL and Reinforcement Learning (RL) for tissue manipulation to estimate the dynamics of an adaptive Model Predictive Control (MPC). They argue that IL works well if the dataset is sufficiently large and that RL is not suited for application on a real robotic system as the learning procedure is too hazardous. Ou et al. [10] address this concern through sim-to-real transfer, by randomizing parameters of the simulation to bridge the physical sim-to-real gap. In our own prior work [4], we employ a learned image translation model to bridge the visual sim-to-real gap for RL of image-based policies for tissue retraction, but require an accurate digital twin of the real setup. In summary, recent work for deformable object manipulation in RAS is divided between RL and IL. IL is the preferred choice for image-based policies, as modeling a digital twin and the resulting sim-to-real gap are still significant hurdles for RL methods. However, the current methods are unable to learn multimodal behaviors and are not sufficiently data efficient. Furthermore, current methods that feature end-to-end learning from observations to end-effector movements do not include strategies to generate gentle motions. MPD is able to address these challenges, learning multimodal behavior from limited data directly from image observations, generating action sequences for gentle manipulation.

Diffusion Policy [2] and BESO [11] present the current state of the art in robotic DIL. Both methods iteratively denoise action sequence samples to generate motion, conditioned on observations. Both works evaluate their methods against multiple state-of-the-art IL methods and find that DIL methods outperform non-diffusion-based methods in terms of success rate, and excel in learning multimodal behaviors. In this work, we investigate Diffusion Policy and BESO under the requirements of RAS and show that MPD addresses the shortcomings of these methods. For tissue dissection, another common task in RAS, Li et al. [12] extend iBC [13] to learn trajectories as a joint distribution of image observations and instrument motions. However, they do not consider transitions between multiple action sequences, as the method predicts actions for short, independent dissection trajectories. From a motion generation perspective of a single, independent action sequence, the method is comparable to Diffusion Policy [2].

Li et al. [14] show that neural networks can be utilized in IL to predict Probabilistic Dynamic Movement Primitive (ProDMP) weight vectors to generate smooth motions with guaranteed initial conditions for planning of consecutive action sequences. However, the method is built on maximizing the log-likelihood of the learned trajectories and is thus unable to model multimodal behaviors. MPD is able to use ProDMPs and model multimodal behaviors through DIL.

III. METHODS

A. Problem Formulation

We predict action sequences $\tau = (\tau_i)_{i=0..n}$ that consist of desired values $\tau_i \in \mathbb{R}^k$ for the next n time steps relative to the current time, where \mathbb{R}^k is a k -dimensional task space. Depending on the task, the task space consists of k actuation Degree of Freedoms (DoFs) such as grasper articulation, and rotations and translations of surgical instruments in relation to a remote center of motion. The action sequences are predicted based on observations $o = (o_j)_{j=-m+1..0}$ from the previous m time steps. We follow an IL approach and train our models on a dataset \mathcal{D} of human demonstrations d . Each demonstration is a sequence pair $(\tau_i, o_i)_{i=0..N}$ over one full task execution with N time steps. For training, the demonstrations are split into multiple action and observation sequences of lengths n and m , respectively. The demonstrations vary in length and are commonly much longer than the predicted action sequences, $n < N$. We focus on action sequences instead of single actions or full trajectories. Action sequences achieve a balance between reducing the compounding error problem of step-based approaches and the flexibility to adapt to changes that arise in real world scenarios due to variability and uncertainties.

B. Preliminaries on Movement Primitives

MPs are a representation of basic elements for robotic motion that can be combined and modulated to generate complex movements [14]. They provide a framework for representing complex motor skills through simple and parametrizable models. ProDMPs [14] offer a unifying framework that overcomes the weaknesses and combines the strengths of Probabilistic Movement Primitives (ProMPs) and Dynamic

Movement Primitives (DMPs). ProDMPs eliminate the need for costly numerical integration associated with DMPs by utilizing precomputed position and velocity basis functions of the fundamental Ordinary Differential Equation (ODE) that are valid for all trajectories. In ProDMPs, the positions y and velocities \dot{y} of a trajectory are formulated as

$$\begin{aligned} y(t) &= c_1 y_1(t) + c_2 y_2(t) + \Phi(t)^\top \mathbf{w}, \\ \dot{y}(t) &= c_1 \dot{y}_1(t) + c_2 \dot{y}_2(t) + \dot{\Phi}(t)^\top \mathbf{w} \end{aligned} \quad (1)$$

where y_1 and y_2 are the two linearly independent complementary functions of the ProDMP’s homogeneous ODE. \dot{y}_1 , \dot{y}_2 are their respective time derivatives. The coefficients c_1 and c_2 are constants derived from the boundary conditions of the ODE. The coefficients are calculated from desired position and velocity at a specific time step, allowing for smooth transitions between action sequences, which is not possible with ProMPs. The basis functions for position and velocity, Φ and $\dot{\Phi}$, are computed once and then used as fixed functions. The weights \mathbf{w} are a composite vector that merge the DMP’s original weight vector with the goal attractor to which the ODE converges. For simplicity, Eq. (1) is shown for a single DoF instead for the full multi-DoF formulation. ProDMPs facilitate planning smooth trajectories with guaranteed boundary conditions while minimizing computational demands.

C. Preliminaries on Score-based Diffusion Models

The two most prominent methods in DIL follow different diffusion frameworks. Diffusion Policy [2] builds on the Denoising Diffusion Probabilistic Models (DDPMs) framework [15] that focuses on reversing the diffusion process at discrete noise levels, relying on probabilistic modeling of the process as a Markov chain. In contrast, BESO [3] builds on the Score-Based Generative Model (SGM) framework that describes the diffusion process as a time-continuous Stochastic Differential Equation (SDE) and learns the gradient of the log probability density, *i.e.*, the score, of the data distribution. In contrast to the DDPM framework, SGM allows for modular selection of critical components such as the noise schedule and numerical solver [16] and is often computationally less expensive [11]. Both frameworks are capable of representing multimodal distributions of action sequences [2], [3].

For MPD, we adopt the SGM framework and closely follow the conventions proposed in [16] and [11]. The diffusion process is modelled as a Probability Flow ODE

$$d\tau = -\dot{\sigma}(t)\sigma(t)\nabla_\tau \log p(\tau|o, \sigma(t)) dt \quad (2)$$

in time t , with score function $\nabla_\tau \log p(\tau|o, \sigma(t))$ as the gradient of the conditional probability p of action sequences τ under observations o and noise schedule $\sigma(t)$. Here, time t is the time of the Probability Flow ODE that describes the diffusion process and not the time that governs the action sequence. To differentiate between the two, we use the subscript i to refer to time steps of an action sequence τ .

The score function is approximated as

$$\nabla_\tau \log p(\tau|o, \sigma(t)) \approx \frac{D_\theta(\tau, o, \sigma(t)) - \tau}{\sigma(t)^2}, \quad (3)$$

where D_θ is a learned denoiser function with weights θ . Applying this approximation to the Probability Flow ODE under a commonly used linear noise schedule $\sigma(t) = t$ yields

$$d\tau \approx \frac{\tau - D_\theta(\tau, o, t)}{t} dt. \quad (4)$$

To further increase modularity of components and enhance performance across different noise magnitude levels, the denoiser D_θ is represented as

$$D_\theta(\tau, o, t) = c_{\text{skip}}(t)\tau + c_{\text{out}}(t)F_\theta(c_{\text{in}}(t)\tau, o, c_{\text{noise}}(t)) \quad (5)$$

with a learnable inner model F_θ and preconditioning by noise dependent functions $c_{\text{skip}}(t)$, $c_{\text{out}}(t)$, $c_{\text{in}}(t)$ and $c_{\text{noise}}(t)$ [16].

The model D_θ is trained with denoising score matching [17] to minimize the loss function

$$\mathbb{E}_{\tau, t, \eta} \left[\left\| \frac{D_\theta(\tau + \eta, o, t) - \tilde{\tau}}{t^2} - \nabla_{\tau + \eta} \log q(\tau + \eta | \tau) \right\|_2^2 \right] \quad (6)$$

with Gaussian noise $\eta \sim \mathcal{N}(0, t^2 I)$ and a noise distribution q . The values of $t \sim v$ are sampled from a distribution v , commonly a logistic distribution [3]. Assuming a Gaussian distribution q and noised sample $\tilde{\tau} = \tau + \eta$, substituting Eq. (3) in Eq. (6) results in the loss

$$\mathbb{E}_{\tau, t, \eta} \left[\left\| \frac{D_\theta(\tilde{\tau}, o, t) - \tau}{t^2} \right\|_2^2 \right]. \quad (7)$$

During inference, new samples of distribution p are generated by gradually denoising samples of a unit Gaussian by following the approximated score function. This is done by solving the Probability Flow ODE with common ODE solvers such as Euler’s method or solvers that are specifically designed for fast inference in diffusion [18].

Training for IL in robotics involves using observations o and corresponding action sequences τ to learn an approximation of the data distribution’s score function. During inference, new action sequences are generated by initially taking a random sample from a standard Gaussian distribution. This sample is refined through the Probability Flow ODE using an ODE solver. This process involves iteratively updating the sample by passing it to the model conditioned on the observation.

D. Movement Primitive Diffusion

We propose MPD, to combine the advantages of SGMs and ProDMPs. In MPD, the inner model F_θ of Eq. (5) consists of a trainable model E_θ that outputs a weight vector \mathbf{w} . Combined with initial values s_0 for position and velocity, \mathbf{w} is decoded into an action sequence τ using a ProDMP. Conceptually, model E_θ denoises an action sequence conditioned on observations and maps it into the ProDMP weight space. The ProDMP acts as a decoder model to map the denoised weights back into action sequence space. The architecture of F_θ is illustrated in Figure 1. The preconditioning functions of Eq. (5) match the context of action generation with MPs. In Diffusion Policy, the network output is the noise that is removed from the sample in one diffusion step. For BESO, the network output is a fusion of absolute sample values and noise. However, for MPD, the inner model output is generated by a

ProDMP that directly outputs trajectory values, so $c_{\text{skip}}(t) = 0$ and $c_{\text{out}}(t) = 1$ are adapted accordingly. The parameters

$$c_{\text{noise}}(t) = \log(t)/4, \quad c_{\text{in}}(t) = 1/\sqrt{t^2 + \sigma_d^2} \quad (8)$$

with $\sigma_d = 0.5$ are identical to the values in [16] and [3].

Robot control benefits from utilizing fine-grained high-frequency action sequences. In DIL, the input and output sizes of the learned model are determined by the number of elements in the denoised action sequence. Using high-frequency action sequences for a fixed time window has a substantial impact on model size. To manage this complexity, action sequences are commonly predicted at a lower frequency, followed by upsampling through interpolation techniques or MPC [2]. However, MPD uses ProDMPs that can predict action sequences at arbitrary frequencies. MPD diffuses a low-frequency action sequence to shape the encoded ProDMP weights. At the final diffusion step, the encoded weight vector is decoded into a high-frequency action sequence for fine-grained robot control. This allows for fewer values in the action sequences during diffusion and further decouples the frequency of demonstration data from predicted action sequences.

A naive alternative to MPD is to diffuse action sequences in the ProDMP's weight space to approximate the score function of weight vector distribution $v(w|o, \sigma(t))$ instead of action sequence distribution $p(\tau|o, \sigma(t))$. In preliminary experiments, we found that diffusing in weight space does not reach the high success rates of diffusing action sequences directly. Diffusing action sequences can leverage sophisticated network architectures such as transformers that benefit from the sequential nature of action sequences, which are not explicit in weight space. MPD thus focuses on diffusing action sequences directly.

MPD generates smooth, multimodal, high-frequency action sequences with guaranteed initial conditions for position and velocity. Utilizing ProDMP helps modeling temporal correlations between actions, which increases data efficiency and generates motions that are suitable for gentle manipulation of deformable objects. MPD builds on the SGM framework and learns to estimate the score function of the data distribution that governs the demonstration data.

IV. EXPERIMENTS

A. Tasks

In our experiments, we evaluate how MPD performs to align with requirements for application in RAS, based on success rate, motion quality, and data efficiency. MPD is evaluated on four different simulated LapGym [19] tasks and their respective real world robotic setups, illustrated in Figure 2. The tasks represent different types of motion such as cooperation of instruments, grasping, and deformable object manipulation, all of which are crucial for successful application in RAS.

In Grasp Lift Touch (GLT), two laparoscopic instruments are controlled to first grasp a gallbladder, lift the gallbladder to expose a target point in the liver's gallbladder bed, and finally touch the target point with an electrocautery hook. The task requires sequential coordination of the instruments as well as grasping and manipulating deformable objects. The

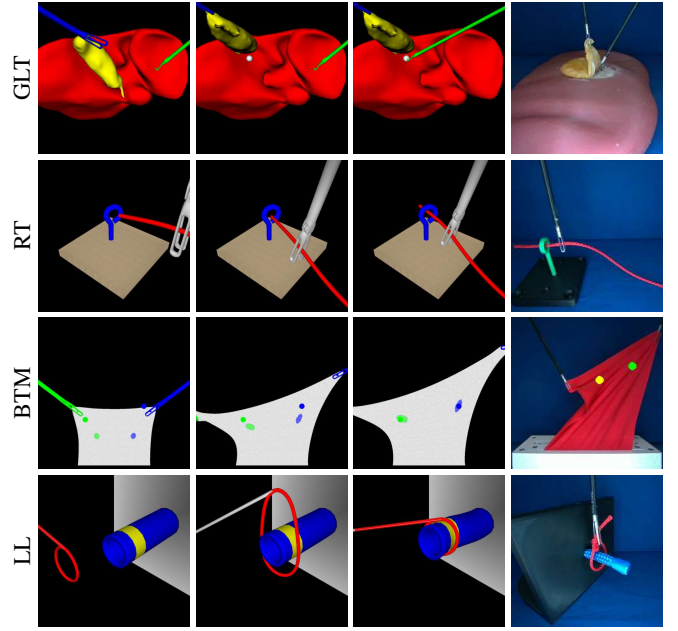


Fig. 2: Start, intermediate, and end state of the tasks in simulation. The final column shows the respective real world experiment. Grasp Lift Touch (GLT) requires sequential collaboration between instruments, Rope Threading (RT) and Ligating Loop (LL) depend on accurate alignment deformable ropes, and Bimanual Tissue Manipulation (BTM) requires concurrent collaboration between instruments to control the shape of a deformable tissue.



Fig. 3: Example images from the real world task. The deformation behavior of the tissue differs significantly from the simulated variant. When stretched, it throws folds and has large variability when slacking without tension, e.g., bulging forward or folding in.

manipulation of the gallbladder is a straightforward retraction motion. The exact deformed shape of the gallbladder plays a subordinate role in exposing the target point as long as the grasped point is sufficiently pulled back.

In Bimanual Tissue Manipulation (BTM), two laparoscopic graspers are attached to the corners of a piece of tissue that is marked with two points. The graspers are controlled to deform the tissue in a way that the two marked points overlap with target points in Cartesian space. In contrast to retraction tasks, this indirect tissue manipulation requires control of the complete shape of the deformable object, and coordination between the instruments is continuous, as motion of any instrument influences the shape of the whole tissue. Both GLT and BTM are characterized by motions that are determined by the instrument's current and target positions.

In Rope Threading (RT), a rope is held by a laparoscopic grasper that is controlled to thread the rope through an eyelet. In contrast to the previous tasks, RT cannot be solved by directly moving the instrument to the target position, but instead has to match waypoints that ensure that the tip of the rope is correctly threaded through the eyelet.

Finally, Ligating Loop (LL) presents a similar challenge but adds further complexity by requiring additional indirect manipulation of a deformable object. In this task, the instrument consists of a rigid shaft and a deformable loop that can be closed to constrict tubular objects, such as blood vessels. The instrument shaft is controlled to maneuver the loop over a tube and constrict the loop around a colored marking. Compared to RT, the loop is much more flexible, deforms more under instrument motion, and requires careful control to navigate a bottleneck of viable waypoints.

The real world tasks replicate the simulated tasks with a setup of xArm7 manipulators (UFactory, China) and laparoscopic graspers (KARL STORZ SE & Co. KG, Germany). RGB images are captured using a D405 camera (Intel RealSense, USA). The spatial resolution from image pixels to Cartesian positions is approximately 1 mm. The real world setup of LL is simplified by omitting the constriction step of the loop. A silicone phantom of a porcine liver with an attached latex gallbladder is used for the GLT setup. The real world setup of BTM uses a piece of 84% polyamid 16% elasthan cloth as tissue and exhibits more complex deformations compared to the simulated task (see Figure 3).

MPD is evaluated against three baselines, namely BESO [3], and two variants of Diffusion Policy [2], DP-C and DP-T. BESO and DP-T are based on transformers, while DP-C employs a 1D temporal CNN model architecture.

B. Evaluation Metrics

Motion Metrics: Applications in RAS have specific requirements for motion behavior in addition to raw success rate of task completion. Tissue acceleration is a metric to quantify surgical performance for gentle manipulation of delicate tissue [20] and should be minimized to reduce risk of tissue damage. We further characterize gentle motions by smooth instrument trajectories. We quantify smoothness based on minimizing instrument jerk to increase safety during motion execution and reduce wear of mechanical components. The motion of skilled surgeons is furthermore characterized by efficient movements [21]. In our work, efficiency is measured by three features, all of which should be minimized: instrument energy as the sum of accelerations over task execution, path length as the travelled distance of the instrument, and episode length as the time to task completion. The five metrics tissue acceleration, instrument jerk, instrument energy, path length, and episode length are evaluated for all tasks, with the following task specific adaptations to represent the metrics. For RT, tissue acceleration is measured as the acceleration of points on the rope. For LL, the instrument consists of a rigid shaft and a deformable loop, so instrument jerk is examined for both parts individually. On the real world tasks, the full state of the tissue is not accessible, so tissue acceleration cannot be measured directly. However, for BTM-RW, marker acceleration is tracked as a surrogate.

Data Efficiency: Data scarcity in the medical domain, particularly in specialized fields such as surgery, requires the development of machine learning methods that efficiently learn from limited data, ensuring reliable applications in clinical

settings. All methods are trained multiple times using varying numbers of demonstrations to evaluate their data efficiency with respect to achieved success rate.

C. Hyper Parameters

Architecture: For all methods, including the baselines, the model architecture parameters are individually optimized during preliminary experiments on BTM as the task is evaluated in simulation and the real world. We found that DP-C performs best with the original values reported in [2] with CNN layer sizes of (256, 512, 1024). BESO, DP-T, and MPD share an optimal transformer architecture, proposed in [2], with 6 layers, 4 heads, attention dropout probability of 0.3 and embedding size of 256.

Observations: All methods are trained for both state and raw RGB image observations. State observations include task-specific state vectors defined in LapGym [19]. Image observations are 256×256 RGB images that are randomly cropped to 224×224 during training and center-cropped during inference. Images are encoded by an adapted ResNet-18 architecture, as described in [2], without pretraining and an output size of 128. For the transformer-based models, the m image observations are encoded independently. For DP-C, the m RGB images are stacked along the color channel before encoding.

Action Sequences: We predict action sequences of length $n = 12$, conditioned on the previous $m = 3$ observations. The time ΔT between both successive observations o_j and successive actions τ_i is 0.1 s. For execution on the real world task, we further generate high-frequency action sequences with $\Delta T = 0.005$ s. The baseline methods require upsampling to calculate the high-frequency action sequences. Linear interpolation is selected for simplicity and computational effectiveness. MPD does not require upsampling, as generating high-frequency action sequences is directly supported by ProDMPs.

Diffusion: Diffusion hyper parameters for the baselines, such as beta schedule and ODE solver, are set according to the respective works. Through initial experiments, we found that Diffusion Policy requires significantly fewer diffusion steps during inference than used during training. We train Diffusion Policy with 100 diffusion steps, and use 5 and 10 diffusion steps during inference for DP-T and DP-C, respectively, without loss of performance. This greatly improves execution time, as only a fraction of model forward passes are required during inference. For MPD we use Euler’s method as the ODE solver, as more sophisticated samplers did not show noticeable improvements. For the ProDMP we use 3 basis functions.

Training: The number of training demonstrations in the datasets are $|\mathcal{D}_{\text{GLT}}| = 90$, $|\mathcal{D}_{\text{RT}}| = 200$, $|\mathcal{D}_{\text{BTM}}| = 150$, $|\mathcal{D}_{\text{LL}}| = 135$, $|\mathcal{D}_{\text{BTM-RW}}| = 200$, and $|\mathcal{D}_{\text{GLT-RW}}| = |\mathcal{D}_{\text{RT-RW}}| = |\mathcal{D}_{\text{LL-RW}}| = 45$. All demonstrations are captured at 10 Hz by a single proficient human demonstrator with an Xbox One controller (Microsoft Corp., USA). MPD and the baseline methods are evaluated every 100 training epochs for 100 task executions. Each method is trained on $r = 5$ random seeds for 3000 epochs. The motion metrics defined in subsection IV-B are aggregated on the individual training run’s epoch that achieved the highest success rate to allow for an accurate

TABLE I: Success rate mean and standard deviation across all simulation tasks based on 5 trained models and 100 rollouts. The best method is **bold**, the second best underlined.

	GLT	RT	BTM	LL	Average
State Observations					
BESO	68.4 (6.8)	<u>90.4</u> (1.2)	88.2 (3.9)	83.2 (4.8)	82.55
DP-T	100 (0.0)	89.6 (1.9)	<u>98.4</u> (0.5)	100 (0.0)	<u>97.00</u>
DP-C	100 (0.0)	82.0 (2.3)	93.2 (1.9)	100 (0.0)	<u>93.80</u>
MPD	<u>99.2</u> (0.7)	93.8 (1.2)	99.0 (0.6)	<u>99.6</u> (0.5)	97.90
Image Observations					
BESO	<u>99.8</u> (0.4)	66.8 (2.3)	91.4 (2.4)	<u>99.8</u> (0.4)	89.45
DP-T	100 (0.0)	76.6 (4.5)	<u>95.8</u> (0.7)	<u>99.8</u> (0.4)	<u>93.05</u>
DP-C	100 (0.0)	83.2 (1.2)	85.2 (1.3)	100 (0.0)	92.15
MPD	100 (0.0)	<u>78.6</u> (3.4)	99.0 (1.1)	100 (0.0)	94.40

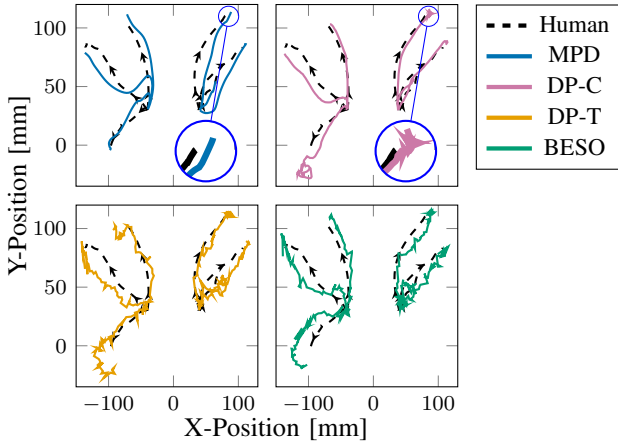


Fig. 4: Cartesian instrument positions of trajectories generated in reference to human demonstrations on the simulated Bimanual Tissue Manipulation task. In contrast to the baselines, MPD consistently generates smooth trajectories.

comparison of each method’s capability by considering its best-case performance scenario.

We use AdamW [22] as optimizer with learning rate, betas, and weight decay as described in [2]. The real world tasks are evaluated using a fully trained model on 50 task executions.

V. RESULTS

Success Rate: Table I reports the success rates for all methods evaluated on the simulation tasks. MPD outperforms the baseline methods with average success rates of 97.9% and 94.4% for state and image observations. DP-T is the second best, reaching 97.0% and 93.05%, respectively. MPD and DP-T further show more consistent performance over different runs compared to the other methods. BESO consistently reaches higher success rates on image observations compared to state observations, while the other methods perform better on state observations. Yet, BESO is still outperformed by the other methods on image observations.

On the real world task, only MPD and DP-C are evaluated. Even though DP-T and BESO outperform DP-C on the simulated BTM task, we do not evaluate them on the real world tasks because the generated action sequences were not gentle enough for execution on the real robot without significant post-processing. Figure 4 illustrates generated trajectories of all methods on the simulated BTM task. Consistent with

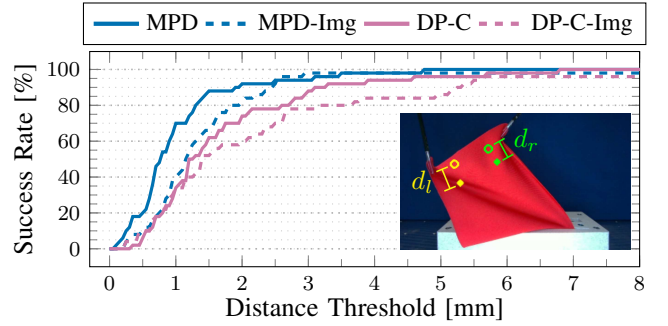


Fig. 5: Success rate of state- and image-based policies on the real world BTM task in relation to the distance threshold T between marker and target.

the motion metric results described below, DP-T and BESO generate considerably jagged action sequences. MPD and DP-C generate overall smooth motion, however, DP-C often shows some jaggedness at the end of the task. On the simulated BTM task, success is defined by a fixed accuracy of aligning the markers and targets. However, in surgical scenarios the desired accuracy is often situational and changes across interventions and surgical phases [23], [24]. Thus, for the real world BTM task, success rate is not reported as a single value, but determined in relation to the desired accuracy for aligning target and marker points. The results for success rate in relation to desired accuracy are shown in Figure 5. The trajectory is successful if the distances d_l and d_r between left and right markers and targets are both below a threshold. MPD outperforms DP-C for both image and state observations up to 6.5 mm accuracy, after which both reach 100% success rate. For 2 mm accuracy and state observations, MPD reaches 90% while DP-C reaches 70% success rate. The success of an episode on the real world RT-RW, LL-RW, and GLT-RW tasks is evaluated manually. Both MPD and DP-C reach 100% success rate on the real world tasks, with the exception of a success rate of 96% for MPD on RT-RW.

Data Efficiency: All methods are trained multiple times using varying numbers of demonstrations. After capture, the demonstrations are shuffled once to mitigate the impact of possible learning curves in the demonstrations. For the experiments, the first x demonstrations are used for training. The results for BTM and RT tasks with state observations are shown in Figure 6. Compared to the baselines, MPD requires much fewer demonstrations to reach high success rates. There is no clear trend as to which baseline method is more data efficient. For BTM, MPD achieves around 90% success rate for 90 demonstrations. The other methods require 120 for DP-T and 200 for DP-C and BESO to reach similar success rates.

Motion Metrics: We evaluate the methods as described in subsection IV-C on the motion metrics defined in subsection IV-B on image observations and present the results in Figure 7. The values are normalized by human demonstration data, so values below 1.0 indicate better-than-demonstrator motion quality. The transformer-based methods, namely BESO and DP-T, show high values for all motion quality metrics, except for episode length. Compared to BESO, DP-T differs noticeably across different runs, with min and

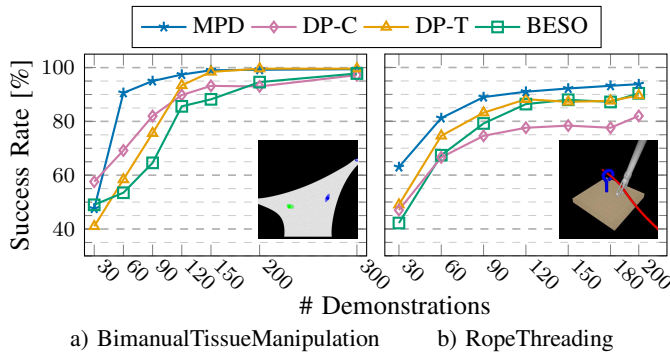


Fig. 6: Success rates of MPD and the baselines over the number of training demonstrations on the Bimanual Tissue Manipulation and Rope Threading tasks on state observations.

max values that deviate far from the mean, see *e.g.*, tissue acceleration in Figure 7 b). We report min and max values for the motion metrics instead of the standard deviation to highlight best- and worst-case scenarios for the methods. The results across different runs are more bounded for MPD and DP-C, with min and max values closer to the mean. DP-C and especially MPD achieve gentle motions whose values are much closer to the human demonstrations on all metrics. MPD performs best across all metrics except for episode length on RT. Using ProDMPs, MPD generates motions that have noticeably less instrument jerk, even compared to human demonstrations.

VI. DISCUSSION

High success rates of image-based policies are crucial for advancing the level of automation in RAS, because image observations are readily available in real surgical settings and do not require complex, task-specific feature extraction to generate state observations [4]. However, we evaluated MPD on both image and state observations to show that the benefits of our method are not limited to image observations. All investigated imitation learning methods reach much higher success rates on the same tasks, compared to policies trained with RL, reported in [19]. However, within the baseline methods there seems to be a trade-off between execution speed, success rate, and motion quality. DP-T, as a transformer-based DDPM baseline reaches the highest baseline success rates, but generates motions that are unfavorable under surgical quality metrics. DP-C employs a 1D temporal CNN model architecture that generates smoother motions compared to the transformer-based baselines. However, the method does not explicitly prevent jagged motions and is noticeably slower during inference. Training speed is mainly influenced by the model architecture. For 3000 epochs, the transformer-based methods require 400 minutes while DP-C requires 200 minutes on average for the real world datasets on a RTX 4090 GPU. In our experiments, training usually converges at around 400 epochs, enabling training in less than an hour. MPD and BESO benefit from the SGM diffusion framework and can be executed with 90 Hz. With the same architecture, DP-T reaches 80 Hz while DP-C reaches 40 Hz due to a computationally more complex architecture. The SGM framework is

therefore favorable for robotic applications that require online motion generation. However, BESO reaches the lowest average success rate on the evaluated tasks. In contrast to the baselines, MPD features the fast inference time of the SGM framework, the high task success rate of transformer-based methods, and improves on the motion quality of temporal CNN models for gentle manipulation of deformable objects. The gentle motions of MPD are due to the use of ProDMPs but have an advantage over other IL methods that also utilize ProDMPs [14] in versatility, as MPD is able to learn multimodal behaviors.

The main limitation of MPD lies in the limited performance outside of the available demonstration data, a common challenge for IL methods, that may be addressed by continued training with feedback [25]. This limitation is apparent in the two failed episodes of the RT-RW task, where initial threading of the rope failed and bent the rope so severely that the policy could not recover from this state. While the tasks are visually simple, surgically more realistic scenes are not a limitation as the relevant visual features are learned end-to-end.

In preliminary experiments, we observed that the transformer-based methods are considerably more sensitive to their respective hyper parameter choices compared to DP-C. These findings are consistent with the findings of [2]. Compared to BESO and DP-T, MPD was less sensitive to the hyper parameters chosen. Furthermore, we observed that predicting more action steps than are executed, as described in [2], did not perform well on the tasks in this work.

MPD further outperforms all baselines in data efficiency, requiring fewer demonstrations to reach high success rates. The baseline methods exhibit a slight decrease in performance when increasing demonstrations from 150 to 180 on the RT task, as shown in Figure 6 b). This result may indicate that, compared to the baselines, MPD performs better when added demonstrations introduce additional modes into the training data or that MPD performs better on suboptimal demonstrations. Future work may investigate the behavior of MPD under these two aspects.

VII. CONCLUSION

This work proposes MPD, a novel method for learning robotic manipulation of deformable objects in the context of RAS. MPD combines the versatility of DIL with the motion quality of ProDMPs, facilitating gentle manipulation of deformable objects and data efficient training that are crucial for surgical applications. The experiments show the superior performance of MPD over traditional DIL methods. MPD achieves higher success rates and further requires fewer demonstrations to reach comparable success rates. MPD shows favorable motion qualities, thereby aligning closely with the requirements for gentle tissue manipulation in surgical settings. The integration of ProDMPs allows generating smooth, high-frequency action sequences with guaranteed initial conditions, without an increase in inference time, required for application in real world robotic scenarios.

In summary, MPD offers a data efficient, gentle, and robust method for the manipulation of deformable objects in the context of RAS. Its ability to learn from limited data while

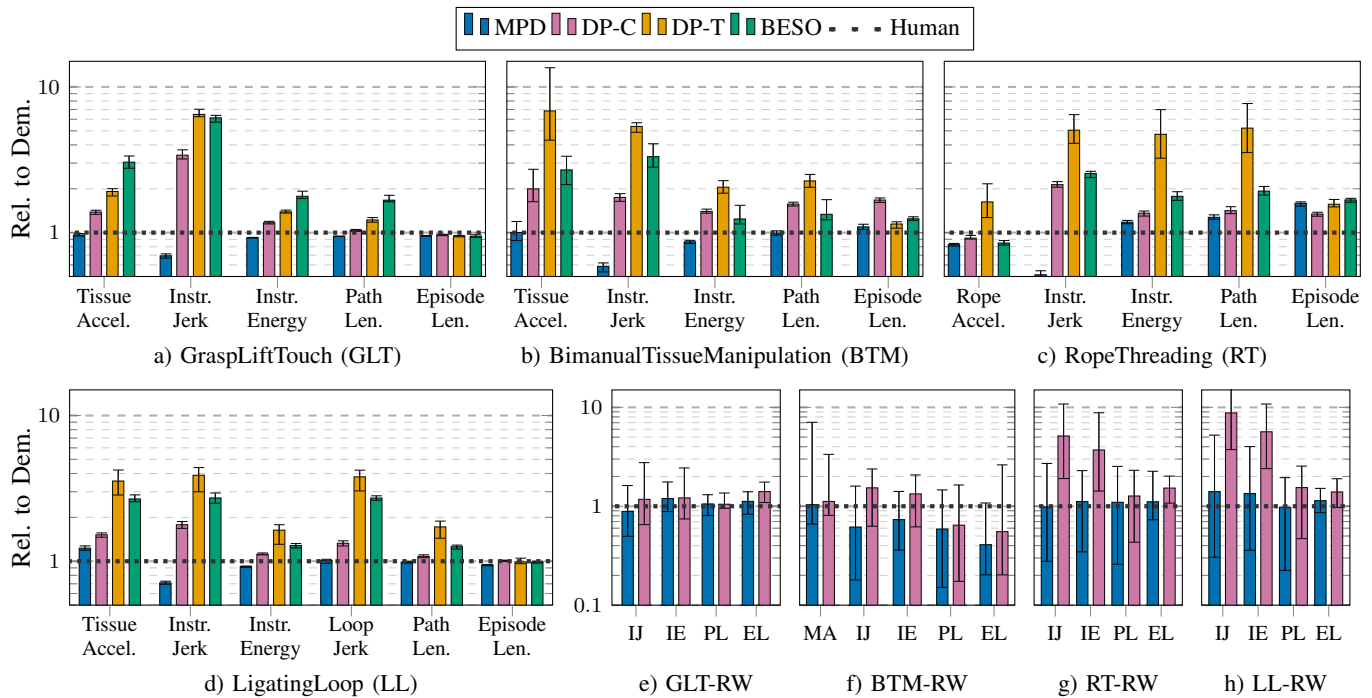


Fig. 7: Motion quality evaluation metrics in relative values to human demonstrations. The bars show the mean value normalized by human demonstration data, with min and max values as error bars. All methods were trained on image observations. MPD consistently outperforms the baselines and exhibits even less Instrument Jerk than the human demonstrations. Real world (RW) tasks e) to h) lack the Tissue Acceleration metric. BTM-RW uses the Marker Acceleration (MA) as a proxy for Tissue Acceleration. Abbreviations: Instrument Jerk (IJ), Instrument Energy (IE), Path Length (PL), Episode Length (EL).

maintaining high-quality motion characteristics makes it a promising approach for future developments in autonomous and semi-autonomous surgical systems. Future research may explore the application of MPD in more diverse surgical scenarios and its integration with other surgical technologies, further pushing the boundaries of robotic assistance in complex medical procedures.

REFERENCES

- [1] D. Blessing, *et al.*, “Information maximizing curriculum: A curriculum-based approach for learning versatile skills,” in *Adv. Neural. Inf. Process. Syst.*, 2023, pp. 51 536–51 561.
- [2] C. Chi, *et al.*, “Diffusion policy: Visuomotor policy learning via action diffusion,” in *Robot.: Sci. Syst.*, 2023.
- [3] M. Reuss and R. Lioutikov, “Multimodal diffusion transformer for learning from play,” in *Conf. Robot. Learn. Workshop*, 2023.
- [4] P. M. Scheikl, *et al.*, “Sim-to-real transfer for visual reinforcement learning of deformable object manipulation for robot-assisted surgery,” *IEEE Robot. Autom. Lett.*, vol. 8, no. 2, pp. 560–567, 2023.
- [5] B. Thach, B. Y. Cho, A. Kuntz, and T. Hermans, “Learning visual shape control of novel 3d deformable objects from partial-view point clouds,” in *IEEE Int. Conf. Robot. Autom.*, 2022, pp. 8274–8281.
- [6] C. Shin, P. W. Ferguson, S. A. Pedram, J. Ma, E. P. Dutson, and J. Rosen, “Autonomous Tissue Manipulation via Surgical Robot Using Learning Based Model Predictive Control,” in *IEEE Int. Conf. Robot. Autom.*, 2019, pp. 3875–3881.
- [7] P. M. Scheikl, *et al.*, “Cooperative Assistance in Robotic Surgery through Multi-Agent Reinforcement Learning,” in *IEEE/RSJ Int. Conf. Intell. Robot. Syst.*, 2021, pp. 1859–1864.
- [8] A. Pore, E. Tagliabue, M. Piccinelli, D. Dall’Alba, A. Casals, and P. Fiorini, “Learning from demonstrations for autonomous soft-tissue retraction,” in *Int. Symp. Med. Robot.*, 2021, pp. 1–7.
- [9] C. D’Ettorre, S. Zirino, N. N. Dei, A. Stilli, E. De Momi, and D. Stoyanov, “Learning intraoperative organ manipulation with context-based reinforcement learning,” *Int. J. Comput. Assist. Radiol. Surg.*, pp. 1419–1427, 2022.
- [10] Y. Ou and M. Tavakoli, “Sim-to-real surgical robot learning and autonomous planning for internal tissue points manipulation using reinforcement learning,” *IEEE Robot. Autom. Lett.*, vol. 8, no. 5, pp. 2502–2509, 2023.
- [11] M. Reuss, M. Li, X. Jia, and R. Lioutikov, “Goal conditioned imitation learning using score-based diffusion policies,” in *Robot.: Sci. Syst.*, 2023.
- [12] J. Li, *et al.*, “Imitation learning from expert video data for dissection trajectory prediction in endoscopic surgical procedure,” in *Int. Conf. Med. Image Comput. Assist. Interv.*, 2023, pp. 494–504.
- [13] P. Florence, *et al.*, “Implicit behavioral cloning,” *Conf. Robot. Learn.*, pp. 158–168, 2021.
- [14] G. Li, Z. Jin, M. Volpp, F. Otto, R. Lioutikov, and G. Neumann, “Prodmp: A unified perspective on dynamic and probabilistic movement primitives,” *IEEE Robot. Autom. Lett.*, vol. 8, no. 4, pp. 2325–2332, 2023.
- [15] J. Ho, A. Jain, and P. Abbeel, “Denoising diffusion probabilistic models,” in *Adv. Neural. Inf. Process. Syst.*, 2020, pp. 6840–6851.
- [16] T. Karras, M. Aittala, T. Aila, and S. Laine, “Elucidating the design space of diffusion-based generative models,” in *Adv. Neural. Inf. Process. Syst.*, 2022, pp. 26 565–26 577.
- [17] Y. Song and S. Ermon, “Generative modeling by estimating gradients of the data distribution,” in *Adv. Neural. Inf. Process. Syst.*, 2019, pp. 11 918–11 930.
- [18] C. Lu, Y. Zhou, F. Bao, J. Chen, C. Li, and J. Zhu, “Dpm-solver: A fast ode solver for diffusion probabilistic model sampling in around 10 steps,” in *Adv. Neural. Inf. Process. Syst.*, 2022, pp. 5775–5787.
- [19] P. M. Scheikl, *et al.*, “LapgyM - an open source framework for reinforcement learning in robot-assisted laparoscopic surgery,” *Journal of Machine Learning Research*, vol. 24, no. 368, pp. 1–42, 2023.
- [20] T. Sugiyama, *et al.*, “Tissue acceleration as a novel metric for surgical performance during carotid endarterectomy,” *Oper. Neurosurg.*, pp. 343–352, 2022.
- [21] P. D. van Hove, G. J. M. Tuijthof, E. G. G. Verdaasdonk, L. P. S. Stassen, and J. Dankelman, “Objective assessment of technical surgical skills,” *Br. J. Surg.*, vol. 97, no. 7, pp. 972–987, 2010.
- [22] I. Loshchilov and F. Hutter, “Decoupled weight decay regularization,” in *Int. Conf. Learn. Rep.*, 2019.
- [23] M. Furuse, *et al.*, “Influence of surgical position and registration methods on clinical accuracy of navigation systems in brain tumor surgery,” *Sci. Rep.*, vol. 13, no. 1, p. 2644, 2023.
- [24] J. Clarke, A. Deakin, A. Nicol, and F. Picard, “Measuring the positional accuracy of computer assisted surgical tracking systems,” *Comput. Aided Surg.*, vol. 15, no. 1-3, pp. 13–18, 2010.
- [25] W. Chi, *et al.*, “Collaborative robot-assisted endovascular catheterization with generative adversarial imitation learning,” in *IEEE Int. Conf. Robot. Autom.*, 2020, pp. 2414–2420.